Adaptive SMC for Lower Limb Rehabilitation Robots Using a Sliding Mode Hyperbolic ESO

Yanlei Yin[1], Aihui Wang[2], Hengyi Li[3], Han Ren[4], Yan Wang[5], Xuebin Yue[6]
{y.yin@zut.edu.cn[1], a.wang@zut.edu.cn[2], lihengyi@zut.edu.cn[3]}

Zhongyuan University of Technology, No. 1 Huaihe Road, Zhengzhou, Henan, 451191, China[1,2,3]

Abstract. In response to the requirements for precision and robustness in trajectory tracking and human-robot interaction of lower limb rehabilitation exoskeleton robots, this paper proposes a sensorless solution that integrates a Sliding Mode Hyperbolic Extended State Observer (SHESO) with Adaptive Sliding Mode Control (ASMC). In this scheme, SHESO is employed to achieve sensorless estimation of external torque disturbances. Compared with the traditional Extended State Observer (ESO), it features a faster convergence speed and a higher estimation accuracy, thereby providing reliable disturbance information for subsequent control. Based on dynamic correction of the desired trajectory by admittance control, the ASMC method further realizes accurate tracking of the corrected gait trajectory and ensures the system stability during human-robot interaction. The stability of both the observer and the controller is rigorously validated via Lyapunov stability theory, while simulation results confirm that the proposed method achieves superior performance in both external disturbance estimation and trajectory tracking.

Keywords: lower limb rehabilitation exoskeleton, sliding mode control, admittance control, sensorless torque estimation, human-robot interaction

1 Introduction

Global aging drives rising demand yet scarce supply of lower-limb rehabilitation, degrading patients' quality of life; lower limb rehabilitation exoskeletons counteract this trend by providing standardized gait training that improves clinical outcomes and reduces the workload of the physician [1, 2]. Current research focuses mainly on passive training, which ignores active participation of patients and may cause adaptability and safety problems [3]. Thus, active training-oriented models are crucial, requiring both high-precision trajectory tracking and human-robot interaction, especially real-time responses to active interaction torque of patients [4].

Admittance control, a mainstream compliant human-robot interaction solution, adjusts trajectories via torque. However, it requires precise torque feedback from physical sensors, increasing system complexity and risking accuracy issues [5]. In recent years, sensorless control methods have become a research focus. Huo et al. [6, 7] used disturbance observers for state estimation, but do not fully investigate convergence speed. Yang et al. [8] proposed a generalized momentum-based

IIKI 2025, December 18-21, Chengdu, People's Republic of China

DOI 10.4108/eai.18-12-2025.2365297

Luenberger observer to estimate the external torque of the end effector. Liu et al. [9] employed an extended state observer (ESO) for internal uncertainties and external disturbances, though sensorless ESO schemes exhibit lag in abrupt disturbance estimation. Traditional ESOs assume disturbances to be slow or constant, which conflicts with the time-varying and discontinuous human-robot interaction torques in rehabilitation training, thereby reducing precision [10].

In the field of robot position control, extensive research has been done on sliding mode control (SMC) methods, which are also widely applied in lower extremity rehabilitation exoskeleton robots [11, 12]. SMC exhibits strong robustness and anti-interference capability, and is typically used in complex nonlinear systems [13]. Yu et al. [14] proposed a terminal SMC, implementing a scheme with finite-time convergence. To further shorten the convergence time, a fast convergence SMC method was put forward [15]. However, the discontinuous reaching law of SMC tends to cause high-frequency chattering, which will aggravate patients' discomfort during rehabilitation training and reduce the compliance of human-robot interaction.

To address the above issues, this paper proposes an ASMC method based on a SHESO. The main contributions are as follows: (1) A sliding mode hyperbolic extended state observer (SHESO) is proposed. Its optimized structure improves the estimation performance of external torque disturbances, achieving faster convergence and higher accuracy. (2) An ASMC with a parameter adaptive mechanism is designe, which balances system stability and trajectory tracking accuracy while effectively tackling time-varying disturbances. (3) A sensorless closed-loop framework is constructed, where SHESO estimates interaction torque online, admittance controller corrects the trajectories, and ASMC allows accurate trajectory tracking.

The following sections of this paper are organized as follows. Section II details the robot dynamics modeling with associated assumptions. Section III describes the design of SHESO, ASMC, and the admittance controller. Section IV verifies the proposed algorithms via simulation. The conclusion is presented in the final section.

2 Preliminaries and robot model description

2.1 Preliminaries

Lemma 1: Let $V(x):\mathbb{R}^n \to \mathbb{R}_{\geq 0}$ be a continuously differentiable positive definite function. If there exist constants $\nu > 0$ and $0 < \vartheta < 1$ such that $\dot{V}(x) \leq -\nu V^{\vartheta}(x)$, then the system states converge to the origin in finite time $T \leq \frac{V^{1-\vartheta}(x(0))}{\nu(1-\vartheta)}$.

2.2 Dynamic Model of Robots

In general, the dynamic model of a lower limb rehabilitation exoskeleton with n degrees of freedom can be written as

$$M(q)\ddot{q} + C(q,\dot{q})\dot{q} + G(q) + \bar{f} = \tau + \tau_{ext} \tag{1}$$

where $q, \dot{q}, \ddot{q} \in \mathbb{R}^{n\times 1}$ are the exoskeleton joint angle, angular velocity, and acceleration vectors; $M(q) \in \mathbb{R}^{n\times n}$ is the inertia matrix; $C(q,\dot{q}) \in \mathbb{R}^{n\times n}$ denotes Coriolis and centrifugal torques; $G(q) \in$

$\mathbb{R}^{n\times 1}$ is the gravity vector; $\tau \in \mathbb{R}^{n\times 1}$ is the joint motor control input; $\tau_{ext} \in \mathbb{R}^{n\times 1}$ represents external interaction torque; and $\bar{f} \in \mathbb{R}^{n\times 1}$ is the lumped disturbance.

This paper adopts a simplified 2 - DOF exoskeleton dynamic model with the following properties:

Property 1: The matrix $M(q)$ is positive definite by virtue of its symmetric structure.

Property 2: The matrix $M(q) - 2C(q,\dot{q})$ is identified as symmetric in skew.

Additionally, the following assumptions hold for system (1):

Assumption 1: The actual states q and $\dot{q}$ of the system are bounded, and the inertia matrix $M(q)$, Coriolis and centrifugal torque matrix $C(q,\dot{q})$ is bounded.

Assumption 2: The lumped disturbance term $\bar{f}$ and its derivative $\dot{\bar{f}}$ both remain bounded, satisfying $\|\bar{f}\| \leq \theta_1$, $\|\dot{\bar{f}}\| \leq \theta_2$.

Assumption 3: In lower limb rehabilitation training, system's model uncertainty is negligible compared to human-machine interaction torque, so this paper assumes that $\tau_{ext} - \bar{f} \approx \tau_{ext}$.

Assumption 4: The derivative of the external torque τ_{ext} of the system is bounded, satisfying $\|\dot{\tau}_{ext}\| \leq L$, $L > 0$.

Define the system state variables

$$x_1 = q, x_2 = \dot{q}, x_3 = \tau_{ext} \tag{2}$$

According to Assumption 3, the system (1) can be redefined within a second-order state-space framework.

$$\begin{cases} \dot{x}_1 = x_2 \\ \dot{x}_2 = M(x_1)^{-1}\big(\tau + x_3 - C(x_1,x_2)x_2 - G(x_1)\big) \\ \dot{x}_3 = \dot{\tau}_{ext} \end{cases} \tag{3}$$

3 Design of controller

3.1 Design of Sliding Mode Hyperbolic Extended State Observer

To achieve safe and compliant human-robot interaction in lower limb rehabilitation, this paper designs a SHESO for interaction torque estimation. Combining sliding mode control advantages with a hyperbolic tangent function, it suppresses high-frequency chattering of the sliding mode observer while retaining strong robustness; additionally, a third-order extended state observer structure enables high-precision estimation of uncertain external torques during rehabilitation.

Firstly, the sliding mode surface of the observer is defined as follows:

$$s_1 = \dot{e_1} + \gamma e_1 \tag{4}$$

where $e_1 = x_1 - \hat{x}_1$ is the angle estimation error; $\hat{x}_1$ is the estimated value of x_1, and γ is a is a positive-definite diagonal matrix.

Then, according to the model (3), the proposed SHESO can be designed as

$$\begin{cases} \dot{\hat{x}}_1 = \hat{x}_2 + \alpha_1 \omega \tanh(s_1) \\ \dot{\hat{x}}_2 = M(x_1)^{-1}\left(\tau + \hat{x}_3 - C(x_1,x_2)\hat{x}_2 - G(x_1)\right) \\ \qquad + \alpha_2 \omega^2 \tanh(s_1) \\ \dot{\hat{x}}_3 = \alpha_3 \omega^3 \tanh(s_1) \end{cases} \tag{5}$$

where $\hat{x}_2$ is the estimated value of x_2; $\hat{x}_3$ is the estimated value of x_3; $\alpha_1, \alpha_2, \alpha_3 > 0$ are the designed observer gain parameters and $\omega > 0$ is the bandwidth parameter.

Define the estimation errors $e_2 = x_2 - \hat{x}_2$, $e_3 = x_3 - \hat{x}_3$. The dynamics of estimation errors can be written as

$$\begin{cases} \dot{e}_1 = e_2 - \alpha_1 \omega \tanh(s_1) \\ \dot{e}_2 = M^{-1}(-Ce_2 + e_3) - \alpha_2 \omega^2 \tanh(s_1) \\ \dot{e}_3 = \dot{x}_3 - \alpha_3 \omega^3 \tanh(s_1) \end{cases} \tag{6}$$

Theorem 1: For system model (1) equipped with the observer designed in (5), if there exists a constant $\varpi > 0$ such that the observer gain satisfies $\kappa \tanh(1) > \eta$, then the sliding surface s_1 will reach the region $P_\varpi = \{s_1 \in \mathbb{R}^n \mid \|s_1\| \le \varpi\}$ in finite time and remain uniformly ultimately bounded.

Proof: Taking the time derivative of the sliding surface s_1 yields

$$\begin{aligned} \dot{s}_1 = {} & M^{-1}(-Ce_2 + e_3) + \gamma e_2 \\ & - \omega(\alpha_2 \omega + \gamma \alpha_1)\tanh(s_1) - \alpha_1 \omega \operatorname{sech}^2(s_1)\dot{s}_1 \end{aligned} \tag{7}$$

Let $\Phi = M^{-1}(-Ce_2 + e_3) + \gamma e_2$. According to Assumption 1 and 4, there exists $\eta > 0$ such that

$$\begin{aligned} \|\Phi\| &\le \|M^{-1}\|\|C\|\|e_2\| + \|M^{-1}\|\|e_3\| + \gamma\|e_2\| \\ &\le \eta_1\|e_2\| + \eta_2\|e_3\| + \gamma\|e_2\| \\ &\le \eta \end{aligned} \tag{8}$$

Rearranging terms gives

$$\dot{s}_1 = \frac{\Phi - \omega(\alpha_2 \omega + \gamma \alpha_1)\tanh(s_1)}{1 + \alpha_1 \omega \operatorname{sech}^2(s_1)} \tag{9}$$

Construct the Lyapunov function

$$V_s = \frac{1}{2} s_1^2 \tag{10}$$

Taking its time derivative yields

$$\dot{V}_s = s_1^{\mathrm{T}} \cdot \frac{\Phi - \kappa(1 + \alpha_1 \omega)\tanh(s_1)}{1 + \alpha_1 \omega \operatorname{sech}^2(s_1)} \tag{11}$$

where $\kappa = \dfrac{\omega(\alpha_2 \omega + \gamma \alpha_1)}{1 + \alpha_1 \omega}$. Since $1 + \alpha_1 \omega \operatorname{sech}^2(s_1) \ge 1$, it follows that

$$\dot{V}_s \le s_1^{\mathrm{T}} \Phi - \kappa s_1^{\mathrm{T}} \tanh(s_1) \tag{12}$$

Furthermore, by applying the Cauchy-Schwarz inequality and substituting (8), we obtain

$$\begin{aligned} \dot{V}_s &\leq \|s_1\|\|\Phi\| - \kappa s_1^{\mathrm{T}} \tanh(s_1) \\ &\leq \eta\|s_1\| - \kappa s_1^{\mathrm{T}} \tanh(s_1) \end{aligned} \tag{13}$$

Take an arbitrary constant $\varpi \in (0,1)$, and consider the region $\Omega_1 = \{s_1 \in \mathbb{R}^n \mid \|s_1\| \geq \varpi\}$. In this region, when $|s_{1,i}| \geq \varpi$, it holds that $s_{1,i}\tanh(s_{1,i}) \geq |s_{1,i}|\tanh(\varpi)$. Therefore,

$$\begin{aligned} s_1^{\mathrm{T}} \tanh(s_1) &= \sum_{i=1}^{2} s_{1,i}\tanh(s_{1,i}) \\ &\geq \sum_{i=1}^{2} |s_{1,i}|\tanh(\varpi) \\ &\geq \|s_1\|\tanh(\varpi) \end{aligned} \tag{14}$$

Substituting (14) into (13) yields

$$\dot{V}_s \leq -\|s_1\|\left(\kappa\tanh(\varpi) - \eta\right) \tag{15}$$

Let $\nu = \kappa\tanh(\varpi) - \eta > 0$. According to Lemma 1 (with $\vartheta = 0.5$), V_s will decrease to the boundary $\|s_1\| = \varpi$ in finite time within Ω_1. That is, there exists a time $T_1 > 0$ such that $\|s_1\| < \varpi$ for all $t \geq T_1$. In the region $\Omega_2 = \{s_1 \mid \|s_1\| < \varpi\}$, from (9), it can be seen that $\dot{s}_1$ is bounded since Φ and $\tanh(s_1)$ are bounded, and $1 + \alpha_1\omega\,\mathrm{sech}^2(s_1) \geq 1$. Therefore, the system states will not diverge to infinity in finite time. Furthermore, at the boundary $\|s_1\| = \varpi$, we have $\dot{V}_s < 0$, which implies that once the system enters Ω_2, it can never leave again. Hence, s_1 always remains within Ω_2, meaning that Ω_2 is a positively invariant set.

In conclusion, the sliding surface s_1 enters the neighborhood P_ϖ in finite time and remains within this neighborhood. Since ϖ can be made arbitrarily small by increasing the gain κ, s_1 can converge to an arbitrarily small neighborhood of the origin.

This completes the proof.

3.2 Design of Admittance Controller

This paper employs a mass-damping-stiffness admittance control model to achieve human-machine interaction control of the exoskeleton. The form of this model is

$$M_d\ddot{e}_f + B_d\dot{e}_f + K_d e_f = -\tau_{ext} \tag{16}$$

where $M_d, B_d, K_d \in \mathbb{R}^{2\times 2}$ stand for mass, damping, and stiffness matrices, respectively, and are all characterized by being positive-definite diagonal matrices. $\tau_{ext} \in \mathbb{R}^{2\times 1}$ is the interaction torque externally applied to the exoskeleton. $e_f = q_d - q_r$ is the error in the admittance correction and $q_d, q_r \in \mathbb{R}^{2\times 1}$ are the input desired trajectory and the reference trajectory corrected by the admittance controller respectively. Through this model, according to the human-robot interaction torque $\hat{\tau}_{ext}$, estimated by the proposed SHESO, the desired trajectory q_d can be reshaped into the admittance reference trajectory q_r, thereby achieving human-machine interaction.

3.3 Design of Adaptive Sliding Mode Controller

To achieve high-precision trajectory tracking and strong robustness against disturbances in lower-limb rehabilitation training, this paper proposes an ASMC scheme combined with SHESO and an admittance control strategy, as illustrated in Fig. 1.

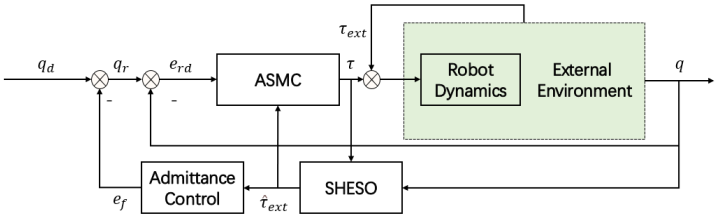

Fig. 1. Algorithm of ASMC System with SHESO and Admittance Controller.

The controller's sliding mode surface is constructed as follows:

$$s_2 = \dot{e}_{rd} + \Lambda e_{rd} \tag{17}$$

where $e_{rd} = q_r - q$, $\dot{e}_{rd} = \dot{q}_r - \dot{q}$, Λ is a positive-definite diagonal matrix and serves as the sliding mode surface gain parameter.

The derivative of the sliding mode surface can be represented as

$$\dot{s}_2 = \ddot{e}_{rd} + \Lambda \dot{e}_{rd} = (\ddot{q}_r - \ddot{q}) + \Lambda \dot{e}_{rd} \tag{18}$$

Based on the proposed SHESO in this paper, the control law is designed as follows:

$$\tau = \tau_{eq} + \tau_{sw} - \hat{\tau}_{ext} \tag{19}$$

where τ_{eq} maintains the system on the sliding mode surface; τ_{sw} suppresses disturbances and unmodeled dynamics; and $\hat{\tau}_{ext}$ is the external torque estimate from SHESO. The equivalent control law and the switching control law are designed as follows:

$$\tau_{eq} = M(q)\ddot{q}_r + C(q,\dot{q})\dot{q}_r + G(q) \tag{20}$$

$$\tau_{sw} = \hat{K} \cdot \mathrm{sgn}(s_2) \tag{21}$$

where $\hat{K} = \mathrm{diag}(\hat{k}_1, \hat{k}_2)$ is a positive-definite diagonal matrix, and $\hat{k}_i$ is the adaptive gain estimation value, updated by the adaptive law (22).

$$\dot{\hat{k}}_i = \mu_i |s_{2,i}| - \sigma_i \hat{k}_i, \quad i = 1,2 \tag{22}$$

where $\mu_i > 0$ is the adaptive gain coefficient and $\sigma_i > 0$ is the correction parameter.

Theorem 2: For system model (1), under the action of the sliding mode control law (19) and the parameter adaptive law (22), all signals of the closed-loop system are uniformly ultimately bounded under bounded initial conditions, and the tracking error converges to a small neighborhood of the origin.

Proof: Choose the Lyapunov function as

$$V = \frac{1}{2} s_2^{\mathrm{T}} M(q) s_2 + \frac{1}{2} \sum_{i=1}^{2} \frac{1}{\mu_i} \tilde{k}_i^2 \tag{23}$$

where $\tilde{k}_i = \hat{k}_i - k_i^*$ $(i = 1,2)$ is the adaptive gain estimation error, and k_i^* is the ideal gain value. Substituting the control laws (19)-(21) into model (1) and rearranging terms yields

$$M\dot{s}_2 = -\hat{K}\,\mathrm{sgn}(s_2) - \tilde{\tau}_{ext} + \bar{f} + (M\Lambda - C)\dot{e}_{\mathrm{rd}} \tag{24}$$

where $\tilde{\tau}_{ext} = \tau_{ext} - \hat{\tau}_{ext}$, which is bounded according to Theorem 1; and $(M\Lambda - C)\dot{e}_{\mathrm{rd}}$ is bounded according to Assumption 1. Taking the time derivative of (23), and substituting (22) and (24), we obtain

$$\dot{V} = -\sum_{i=1}^{2} k_i^* |s_{2,i}| + s_2^{\mathrm{T}} \varphi + \frac{1}{2} s_2^{\mathrm{T}} \dot{M} s_2 + \sum_{i=1}^{2} \frac{\sigma_i}{\mu_i} \hat{k}_i \tilde{k}_i \tag{25}$$

where $\varphi = -\tilde{\tau}_{ext} + \bar{f} + (M\Lambda - C)\dot{e}_{\mathrm{rd}}$ is bounded, satisfying $\|\varphi\| \le \Psi$. From Property 2 and Assumption 1, there exists $\partial > 0$ such that $\|M\| \le \partial$, thus

$$\frac{1}{2} s_2^{\mathrm{T}} \dot{M} s_2 \le \frac{\alpha}{2} \|s_2\|^2 \tag{26}$$

Let $\sum_{i=1}^{2} \frac{\sigma_i}{\mu_i} \hat{k}_i \tilde{k}_i \le \rho$. In addition, let $k_{\min}^* = \min(k_1^*, k_2^*)$, then

$$-\sum_{i=1}^{2} k_i^* |s_{2,i}| \le -k_{\min}^* \|s_2\| \tag{27}$$

Substituting (26) and (27) into (25) yields

$$\dot{V} \le -(k_{\min}^* - \Psi)\|s_2\| + \frac{\alpha}{2}\|s_2\|^2 + \rho \tag{28}$$

Choose $k_{\min}^*$ such that $k_{\min}^* - \Psi > 0$. From (28), it can be seen that $\dot{V} < 0$ when $\|s_2\|$ exceeds a certain threshold. Therefore, $\|s_2\|$ eventually enters and remains in a bounded region, i.e., s_2 is uniformly bounded. Since s_2 is bounded, equation (22) represents a first-order linear system with bounded input, so $\hat{k}_i$ is bounded, and thus $\tilde{k}_i$ is bounded. That is, there exists a constant $\rho > 0$ such that $\sum_{i=1}^{2} \frac{\sigma_i}{\mu_i} \hat{k}_i \tilde{k}_i \le \rho$. From the definition of the sliding mode surface (17), it can be concluded that the tracking error e_{rd} and its derivative eventually converge to a small neighborhood of the origin, and all closed-loop signals are uniformly ultimately bounded.

This completes the proof.

4 Simulation results

To verify the proposed algorithm, this section uses MATLAB/Simulink for simulations to mimic lower limb rehabilitation training. The 2-DOF exoskeleton model in Fig. 2 is adopted, which reproduces key lower limb motion features and provides a realistic physical basis for simulation.

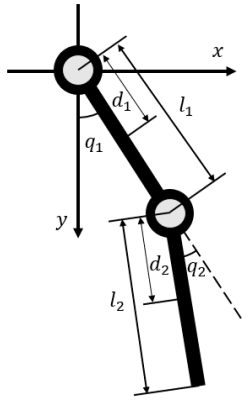

Fig. 2. Single-leg Two-link Model of Lower-limb Rehabilitation Exoskeleton.

The dynamic parameters are as follows:

$$M = \begin{bmatrix} M_{11} & M_{12} \\ M_{21} & M_{22} \end{bmatrix}, \quad C = \begin{bmatrix} C_{11} & C_{12} \\ C_{21} & C_{22} \end{bmatrix}, \quad G = \begin{bmatrix} G_1 \\ G_2 \end{bmatrix} \tag{29}$$

where

$$\begin{cases} M_{11} = m_1 d_1^2 + m_2 l_1^2 + m_2 d_2^2 + 2 m_2 l_1 d_2 \cos q_2 \\ M_{12} = -(m_2 l_1 d_2 \cos q_2 + m_2 d_2^2) \\ M_{21} = -m_2 d_2 (l_1 \cos q_2 + d_2) \\ M_{22} = m_2 d_2^2 \\ C_{11} = (-2 m_2 l_1 d_2 \sin q_2)\dot{q}_2 \\ C_{12} = (-m_2 l_1 d_2 \sin q_2)\dot{q}_2 \\ C_{21} = (m_2 l_1 d_2 \sin q_2)\dot{q}_1 \\ C_{22} = 0 \\ G_1 = -m_1 g d_1 \sin q_1 - m_2 g l_1 \sin q_1 - m_2 g d_2 \sin(q_1 - q_2) \\ G_2 = m_2 g d_2 \sin(q_1 - q_2) \end{cases} \tag{30}$$

m_1, m_2 are the masses of the exoskeleton thigh and shank, respectively. l_1 is the thigh length. d_1, d_2 are the distances from the centers of mass of the thigh and shank to their respective joint centers, and g stands for gravitational acceleration.

In the simulation experiments, the desired trajectory was obtained as follows. An infrared passive optical motion capture system collected a healthy adult motion trajectory [16]. The trajectory

data was then filtered, followed by fitting to obtain Fourier functions of the hip and knee joints, which served as the desired trajectory of the system. Specific expressions are as follows:

$$\begin{aligned}
q_d(1) &= 0.08335 \\
&\quad + 0.002038\cos(0.2174t) - 0.008812\sin(0.2174t) \\
&\quad + 0.04158\cos(0.4348t) + 0.004634\sin(0.4348t) \\
&\quad + 0.04158\cos(0.6522t) + 0.004634\sin(0.6522t) \\
&\quad - 0.1409\cos(0.8696t) + 0.1545\sin(0.8696t) \\
&\quad + 0.04073\cos(1.087t) + 0.04348\sin(1.087t) \\
q_d(2) &= 0.4202 \\
&\quad + 0.02816\cos(0.3142t) - 0.0415\sin(0.3142t) \\
&\quad + 0.0939\cos(0.6284t) - 0.09252\sin(0.6284t) \\
&\quad - 0.2007\cos(0.9426t) + 0.3199\sin(0.9426t) \\
&\quad - 0.08075\cos(1.2568t) + 0.09316\sin(1.2568t) \\
&\quad - 0.03518\cos(1.571t) + 0.2463\sin(1.571t)
\end{aligned} \tag{31}$$

To assess the performance of the SHESO proposed in this paper, an input consisting of a cosine signal embedded with random noise is applied to the system.

$$f(t) = 3\cos(2t) + 0.8 \cdot \begin{cases} Z, & \text{If } U > 0.9 \\ 0, & \text{Otherwise} \end{cases} \tag{32}$$

where $Z \sim \mathcal{N}(0,1)$ is characterized by a standard normal distribution curve and $U \sim \mathcal{U}(0,1)$ is characterized by a uniform distribution over a defined interval. The results are shown in Fig. 3.

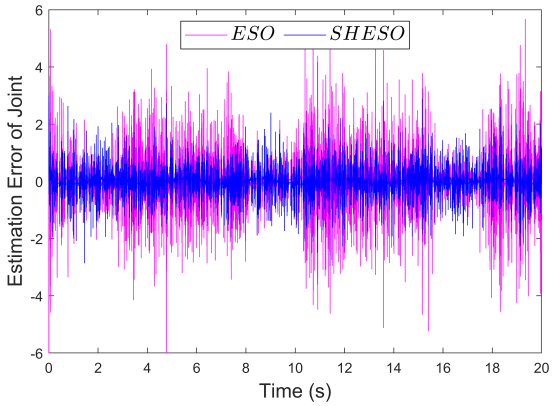

Fig. 3. Estimation Errors of Different Observers.

Table 1: Analysis of Estimation Errors of Different Observers

Error Index	ESO	SHESO
MAE ($\mathrm{N}\cdot\mathrm{m}$)	0.4738	0.1414
RMSE ($\mathrm{N}\cdot\mathrm{m}$)	0.7753	0.2817
MAXAE ($\mathrm{N}\cdot\mathrm{m}$)	12.2111	3.0000
IAE ($\mathrm{N}\cdot\mathrm{m}\cdot\mathrm{s}$)	9.5000	2.8000

It can be clearly seen from Fig. 3 that, compared with the traditional ESO observer, the proposed SHESO in this paper has a smaller estimation error for the external torque. Then, analysis is conducted on the estimation error data, with key indicators including MAE, RMSE, MAXAE, and IAE. The results are shown in Table 1.

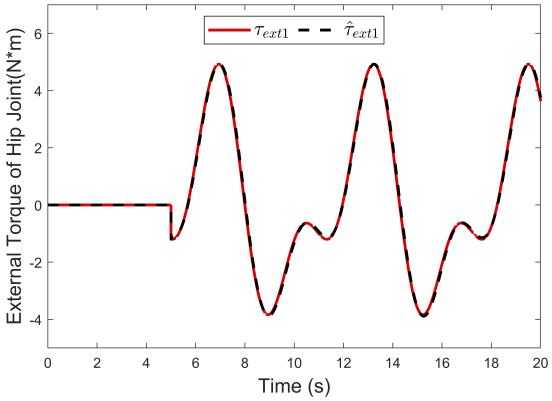

Fig. 4. Estimation of External Torque of Hip Joint.

A comparative analysis of the metrics in Table 1 indicates that the SHESO outperforms the ESO across all critical parameters: its MAE is 70.2% lower, RMSE 63.7% lower, MAXAE reduced by 75.4% and IAE decreased by 70.5%. These results confirm that the SHESO enhances both estimation accuracy and anti-interference capability, particularly excelling in observing sudden disturbances, thus establishing it as a superior state observer design.

Then, to further validate the control efficacy of ASMC, after the system has been running for 5 seconds, white noise signals:

$$\begin{cases} f_1(t) = 3\cos(t) + 2\sin(2t) + \sin(t) \\ f_2(t) = 3\cos(t) + \sin(2t) + 2\sin(t) \end{cases} \tag{33}$$

are introduced. These signals simulate external torque inputs to observe the system's control performance. The parameters of SHESO are: $\gamma = \mathrm{diag}(1,1)$, $\alpha_1 = \mathrm{diag}(3,3)$, $\alpha_2 = \mathrm{diag}(5,5)$, $\alpha_3 =$

$\mathrm{diag}(14,10)$, $\omega = \mathrm{diag}(15,13)$; the parameters of the admittance controller are: $M_d = \mathrm{diag}(0.5,0.5)$, $B_d = \mathrm{diag}(20,20)$, $K_d = \mathrm{diag}(100,100)$; the parameters of ASMC are: $\Lambda = \mathrm{diag}(8,6)$, $\mu_1 = 20$, $\mu_2 = 20$, $\sigma_1 = 0.05$, $\sigma_2 = 0.05$. The experimental results are shown in Figs. 4-9.

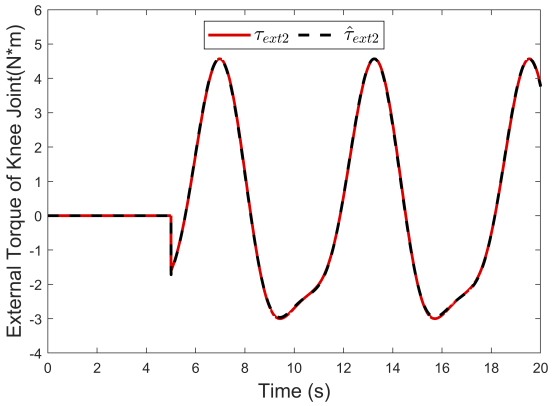

Fig. 5. Estimation of External Torque of Knee Joint.

Figs. 4 and 5 present the estimation effects of the external torques in the hip joint and the knee joint. The analysis shows that, regardless of sudden disturbances or continuous disturbances, the proposed SHESO can achieve accurate estimation of such torques, and the estimation results highly coincide with the actual disturbances, verifying the effectiveness of this observer in complex disturbance scenarios.

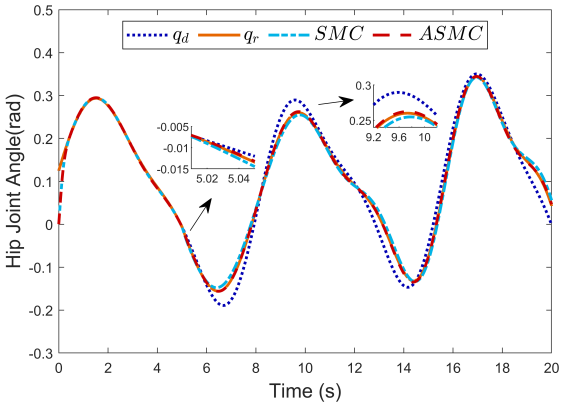

Fig. 6. Trajectory Tracking Effects of Different Controllers for Hip Joint.

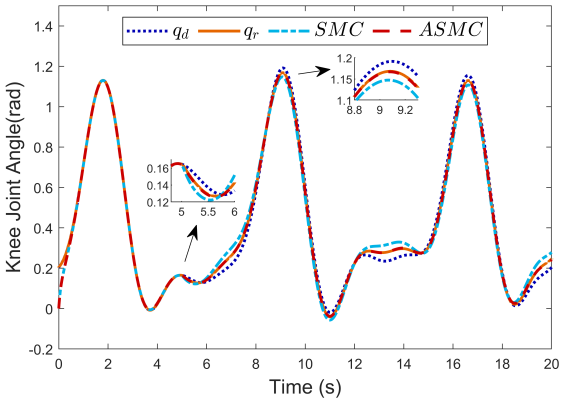

Fig. 7. Trajectory Tracking Effects of Different Controllers for Knee Joint.

As can be seen in Figs. 6 and 7, when the lower limb rehabilitation robot system is subjected to external moments, the admittance controller will dynamically modify the desired trajectory q_d based on the state of human-robot interaction. By perceiving the dynamic changes of the interaction force, it generates an admittance trajectory q_r that matches the actual interaction requirements. On this basis, the ASMC controller can drive the robot to achieve accurate tracking of the admittance trajectory q_r, endowing the human-robot interaction process with favorable compliance characteristics.

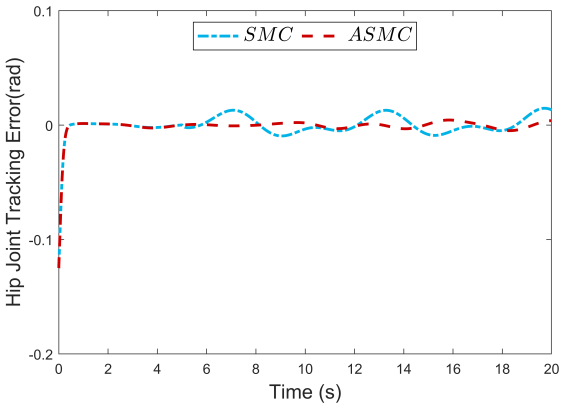

Fig. 8. Trajectory Tracking Errors of Different Controllers for Hip Joint.

Figs. 6-9 show the tracking effects of two control methods. Comparison reveals that the designed ASMC has better tracking accuracy than the traditional SMC. This difference arises because

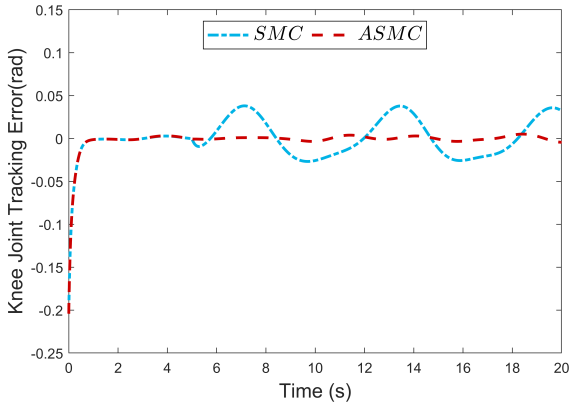

Fig. 9. Trajectory Tracking Errors of Different Controllers for Knee Joint.

the traditional SMC algorithm itself cannot compensate for external disturbances. In contrast, the ASMC estimates and compensates for external interaction torques via an observer, adaptively adjusts parameters, and dynamically suppresses such disturbances.

5 Conclusion

To meet the requirements of high-precision trajectory tracking and compliant human-robot interaction for lower limb rehabilitation exoskeleton robots, this work proposes an Adaptive Sliding Mode Control (ASMC) method based on the Sliding Mode Hyperbolic Extended State Observer (SHESO). In this method, SHESO can estimate external torque disturbances without force sensors, and compared to traditional ESO, it has a faster convergence speed and higher estimation accuracy. In addition, the admittance controller dynamically corrects the desired trajectory according to the human-robot interaction state; ASMC achieves precise tracking of the admittance reference trajectory while ensuring the robustness of the system. The stability of the observer and the controller is verified through Lyapunov stability theory. The simulation results indicate that the proposed SHESO can precisely estimate the external interaction torque exerted by patients during rehabilitation training of the lower limb exoskeleton. Furthermore, the ASMC achieves high-precision trajectory tracking while ensuring a compliant human-robot interaction. However, this study still has certain limitations: it does not fully consider the sampling delay and friction nonlinearity of the actual system, and it ignores the model parameter perturbation caused by individual differences in the human body. Future work will further verify the application feasibility of this method in real rehabilitation scenarios.

Acknowledgments

This research was partially funded by the Henan Province Key Research and Development Project (Grants No. 241111312000), Henan Province Key International Science and Technology Cooperation Project (Grants No. 251111520400), the Key R&D Project of Henan Province (Grants No. 251111220900), and the Henan Province Key Technologies Research Development project (Grants No. 252102211106, 252102320281).

References

[1] Ma Y, Wu X, Yi J, Wang C, Chen C. A review on human-exoskeleton coordination towards lower limb robotic exoskeleton systems. Int J Robot Autom. 2019;34(4):431-51.

[2] Plaschka C, Sawchuck D, Orr T, Bailey T, Waterhouse D, Livingston N. Global policies on assistive robots for care of the elderly: A scoping review. International Journal of Healthcare. 2020;6(1):63.

[3] Cao W, Chen C, Wang D, Wu X, Chen L, Xu T, et al. A Lower Limb Exoskeleton With Rigid and Soft Structure for Loaded Walking Assistance. IEEE Robotics and Automation Letters. 2022;7(1):454-61.

[4] Tu Y, Zhu A, Song J, Shen H, Shen Z, Zhang X, et al. An adaptive sliding mode variable admittance control method for lower limb rehabilitation exoskeleton robot. Applied Sciences. 2020;10(7):2536.

[5] Sebastian G, Li Z, Crocher V, Kremers D, Tan Y, Oetomo D. Interaction force estimation using extended state observers: An application to impedance-based assistive and rehabilitation robotics. IEEE Robotics and Automation Letters. 2019;4(2):1156-61.

[6] Huo W, Alouane MA, Amirat Y, Mohammed S. Force Control of SEA-Based Exoskeletons for Multimode Human–Robot Interactions. IEEE Transactions on Robotics. 2020;36(2):570-7.

[7] Bouakrif F. Trajectory tracking control using velocity observer and disturbances observer for uncertain robot manipulators without tachometers. Meccanica. 2017;52(4):861-75.

[8] Yang C, Peng G, Cheng L, Na J, Li Z. Force Sensorless Admittance Control for Teleoperation of Uncertain Robot Manipulator Using Neural Networks. IEEE Transactions on Systems, Man, and Cybernetics: Systems. 2021;51(5):3282-92.

[9] Liu D, Wang J, Wang S. Force-Sensorless Active Compliance Control for Environment Interactive Robotic Systems. IEEE/ASME Transactions on Mechatronics. 2025;30(2):1481-91.

[10] Han L, Mao J, Cao P, Gan Y, Li S. Toward Sensorless Interaction Force Estimation for Industrial Robots Using High-Order Finite-Time Observers. IEEE Transactions on Industrial Electronics. 2022;69(7):7275-84.

[11] Farbood M, Shasadeghi M, Niknam T, Safarinejadian B. Fuzzy Lyapunov-Based Model Predictive Sliding-Mode Control of Nonlinear Systems: An Ellipsoid Recursive Feasibility Approach. IEEE Transactions on Fuzzy Systems. 2022;30(6):1929-38.

[12] Jallouli-Khlif R, Abdelhedi F, Zayane C, Nouri AS, Derbel N. Robust Sliding Mode Control Based on Fractional Order Reaching Law for Rehabilitation Robots. IEEE Access. 2025;13:75744-53.

[13] Yang B, Yu T, Shu H, Dong J, Jiang L. Robust sliding-mode control of wind energy conversion systems for optimal power extraction via nonlinear perturbation observers. Applied Energy. 2018;210:711-23.

[14] Yu S, Yu X, Shirinzadeh B, Man Z. Continuous finite-time control for robotic manipulators with terminal sliding mode. Automatica. 2005;41(11):1957-64.

[15] Doan QV, Vo AT, Le TD, Kang HJ, Nguyen NHA. A Novel Fast Terminal Sliding Mode Tracking Control Methodology for Robot Manipulators. Applied Sciences. 2020;10(9):3010.

[16] Ren J, Wang A, Li H, Yue X, Meng L. A Transformer-Based Neural Network for Gait Prediction in Lower Limb Exoskeleton Robots Using Plantar Force. Sensors (Basel). 2023;23(14):6547.